Atomic Coherence of 2 Minutes and Instability of 1.5×10^{-18} at 1 s in a Wannier-Stark Lattice Clock

Kyungtae Kim,[1] Alexander Aeppli,[1] William Warfield,[1] Anjun Chu,[1,2] Ana Maria Rey,[1] and Jun Ye[1]
[1]JILA, National Institute of Standards and Technology and the University of Colorado, Boulder, Colorado 80309-0440, USA
and Department of Physics, University of Colorado, Boulder, Colorado 80309-0390, USA
[2]Pritzker School of Molecular Engineering, University of Chicago, Chicago, Illinois 60637, USA

(Received 9 May 2025; revised 11 July 2025; accepted 1 August 2025; published 3 September 2025)

We explore the limits of atomic coherence and measurement precision in a ^{87}Sr optical lattice clock. We perform a detailed characterization of key effects, including lattice Raman scattering and atomic collisions in a shallow lattice configuration, determining a 174(28) s $^3P_0$ clock state lifetime. Investigation of atomic coherence across a range of lattice depths and atomic densities reveals decoherence mechanisms related to photon scattering and atomic interaction. At a reduced density, we observe a coherence time of 118(9) s, approaching the fundamental limit set by spontaneous emission. Guided by this coherence understanding, we demonstrate a clock instability for an atomic ensemble of 1.5×10^{-18} at 1 s in fractional frequency units. Our results are important for further advancing the state of the art of an optical lattice clock for fundamental physics applications.

DOI: 10.1103/3wtv-sty2

Introduction—Optical lattice clocks (OLCs) offer exceptional measurement precision by simultaneously interrogating a large number of atoms with a long coherence time [1–3]. The applications of OLCs range from timekeeping [4] to quantum sensing for fundamental physics [5–8] and are versatile platforms for exploring many-body physics [9–13]. Of fundamental importance in modern quantum science and technology is the scalability of a quantum system, and OLCs provide an ideal platform to explore relevant trade-offs for optimization. The use of many atoms reduces quantum projection noise (QPN) but inevitably introduces atomic interactions as a potential roadblock for both precision and accuracy. Spin squeezing provides a potential solution by providing better signal to noise with fewer atoms [14]. Using an insulating quantum gas in a 3D optical lattice or optical tweezer arrays provides another route for number scaling [15–17]. However, even minute interaction effects such as weak dipolar coupling [12] or superexchange spin interactions [13] can noticeably affect clock operation. In a 1D Wannier-Stark lattice, we have engineered the interaction Hamiltonian to overcome the trade-off between systematics and the atom number [18]. These efforts share a common goal: to realize atomic coherence time limited by fundamental spontaneous emission while employing as many atoms as possible.

One major limitation to the observed coherence time in ^{87}Sr clock transition arises from Raman scattering of the lattice photons for individual atoms [19–21]. This process leads to a reduction in the contrast of Ramsey spectroscopy [22]. The other source of decoherence is atomic interactions [23]. Although a large number of atoms N is desired to reduce QPN, it degrades the coherence time through atomic interactions. A large beam waist, gravity-induced Wannier-Stark 1D optical lattice [24] allows us to operate the clock at a lattice depth of only a few photon recoil energy E_r, which greatly reduces the lattice photon scattering as well as atomic density.

Previously, we investigated how the spin-orbit coupling [10,25] in a Wannier-Stark OLC introduces off site s-wave interaction [18]. Near a specific optical lattice depth $U_0 \sim 10E_r$, we null the mean interaction strength, enabling us to utilize a large N without losing metrological precision. This is essential for resolving sub-mm gravitational redshift [6] and reducing systematic uncertainties [26,27]. A natural next step is to explore how these interactions affect the coherence time.

In this Letter, we study the effect of lattice light scattering and atomic collisions on clock performance for different lattice depths and demonstrate an atomic coherence time of ∼2 min. Raman scattering leads to population accumulation in different nuclear spin states of $^1S_0$. The resulting "spectator" atoms collide via strong s-wave interactions with those in clock states, dominating the decoherence rate. With *in situ* imaging [28] of the atomic distribution, we infer the coherence time by extrapolating to a zero density limit. When this limit is further extrapolated to $U_0 = 0$, we find that the atomic decoherence is in agreement with the limit set by the natural lifetime of $^3P_0$ and blackbody radiation (BBR) from the environment. Furthermore, we use this system to investigate the intrinsic clock precision and demonstrate an instability of 1.5×10^{-18} at 1 s.

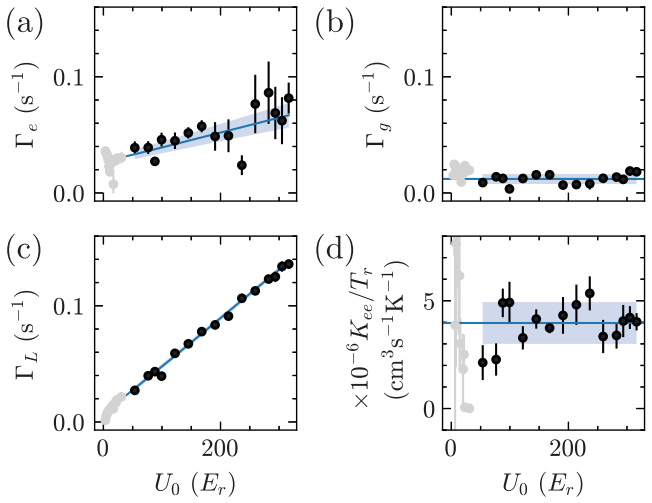

FIG. 1. Lattice depth dependent population decay rates. (a) Single-body loss rate of the excited state. (b) Single-body loss rate of the ground state. (c) $e \to g$ pumping rate. (d) Two-body loss rate of the excited state. Each horizontal axis represents the peak lattice depth, U_0. We use the lattice depth greater than the $50E_r$ (black markers) for the fit (see text). The extracted coefficients are summarized in Table I. The error bars show the 68% confidence interval. The blue lines are fitted curves, and the shades are their uncertainties.

Detailed description of the experimental apparatus can be found in Refs. [6,18,27]. Notably, the trap lifetime is improved by more than a factor of 8 in our recent work [27], which allows us to explore longer timescales with greater signal-to-noise ratio. We prepare the atoms in $|^1S_0 \equiv g, m_F = -5/2\rangle$ at $U_0 = 20E_r$. For the population decay measurement, we use a π pulse to populate $|^3P_0 \equiv e, m_F = -3/2\rangle$ and remove the remaining population in $|g\rangle$ using a strong $^1S_0 \leftrightarrow {}^1P_1$ transition at 461 nm. Then, we adiabatically ramp the lattice to the desired U_0 in 50 ms and hold it with a variable time and measure the atomic population. To measure the coherence time of the clock transition, $|g, m_F = -5/2\rangle \leftrightarrow |e, m_F = -3/2\rangle$, we observe the contrast of the Ramsey fringe with the varying dark time. Finally, we use the imaging spectroscopy method [28] to estimate the frequency measurement noise contributed by the atoms.

Population decay—Environmental perturbations, such as lattice photon scattering, can extract information from an atom [29,30], and consequently any state-dependent perturbation can cause decoherence of the clock superposition. For example, half of the $e \to g$ decay rate directly contributes to the decoherence rate. The use of a magic wavelength in OLCs protects coherence by removing the information carried out by the photon [19,20], as well as minimizing the effect from atomic motion. State-independent trap loss does not directly affect the coherence time, but it can have an indirect impact by requiring an increase of the initial N to achieve a reasonable signal to noise at the detection stage.

TABLE I. Summary of the population decay rate measurement. U is average lattice depth (see text for the details) in units of $E_r = (h/\lambda_L)^2/2M \approx h \times 3.57$ kHz, where h is Planck constant, λ_L is the magic wavelength (813.427 nm) [26], and M is the mass of ^{87}Sr.

Quantity	Value
$\Gamma_e(U)$	$(1.3(3) \times 10^{-4} U/E_r + 2.7(4) \times 10^{-2})$ s^{-1}
Γ_g	$1.2(4) \times 10^{-2}$ s^{-1}
$\Gamma_L(U)$	$(4.30(7) \times 10^{-4} U/E_r + 8.1(8) \times 10^{-3})$ s^{-1}
K_{ee}/T_r	$4(1) \times 10^{-6}$ cm^{-3} s^{-1} K^{-1}
$1/\Gamma_{\text{nat}}$	174(28) s

The population dynamics of the atoms in the optical lattice can be described by the following rate equation:

$$\dot{N}_e = -\Gamma_e N_e - \Gamma_L N_e - K_{ee}/v N_e^2,$$
$$\dot{N}_g = -\Gamma_g N_g + \Gamma_L N_e, \quad (1)$$

where $N_{e(g)}$ is the atom number per site in $|e(g)\rangle$, $\Gamma_{e(g)}$ is the single-body loss rate for $e(g)$, and $K_{ee} \propto T_r$ is the two-body loss rate of $|e\rangle$, where T_r (assumed to be time independent) is the radial temperature [31], and $v(T_r, U_0)$ is the effective volume per site. $\Gamma_L(U) = \Gamma_L(0) + (\partial_U \Gamma_L)U$ is the rate for $e \to g$. $U = \eta(1)U_0 - \eta(1/2)\sqrt{U_0 E_r}$ is the averaged lattice depth, with $\eta(j) = (1 + jk_B T_r/U_0 E_r)^{-1}$ and k_B the Boltzmann constant [26,32]. To extract the decay rates, we measure the population dynamics starting in $|e\rangle$ and fit Eq. (1) to the data using a least-squares method.

Figure 1 and Table I present the measurement results. For the fit, we use lattice depths greater than $50E_r$ (black markers) to exclude the loss effects from parametric heating and Raman scattering recoil, which become significant at shallower depths in our experiment.

Raman scattering drives $^3P_0$ population into the $^3P_1$ and $^3P_2$ states [20], and then the $^3P_1$ state quickly decays to the $^1S_0$ state with a rate Γ_L. The value of $\Gamma_L(0) = 8.1(8) \times 10^{-3}$ s^{-1} represents the limit set by the combined effect of the spontaneous decay of $^3P_0$ and the BBR scattering rate. After subtracting the contribution of the BBR of 2.36×10^{-3} s^{-1} [20,27,33], we obtain a lifetime of the $^3P_0$ state of $1/\Gamma_{\text{nat}} = 174(28)$ s. This is in agreement with previous measurements [20,34,35] and is longer than reported in [36].

Γ_g shows no dependence on U_0, suggesting the background gas collision as the dominant $|g\rangle$ loss mechanism. On the other hand, Γ_e shows a linear dependence on U. We attribute this dependence to the Raman scattering into $^3P_2$, which has a large inelastic cross section with the clock states. The ratio of the background gas collision rates, $\Gamma_e(0)/\Gamma_g$ of 2.3(8), is slightly larger than the values of 1.1 reported in Refs. [20,21], which are obtained under fairly

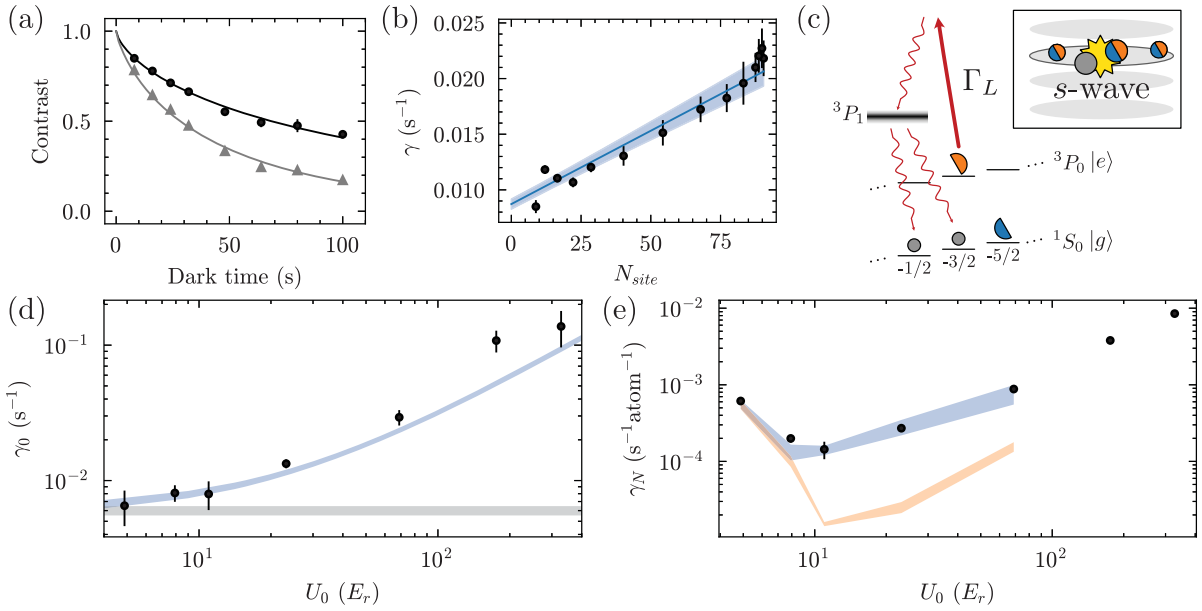

FIG. 2. Collisional interactions and the atomic coherence time. (a) Contrast of the Ramsey fringe as a function of the dark time for two different mean atom numbers per site cases. The circle (triangle) is for $N_{\text{site}} = 9(90)$. Solid lines are a fit to a stretched exponential model. The coherence time, γ^{-1} for $N_{\text{site}} = 9$ is 118(9) s at $11E_r$. (b) Density dependence of the contrast decay rate. The blue solid line is a fit to a linear curve. (c) A cartoon illustrates the generation of spectator atoms (gray) via the lattice Raman scattering. The semicircles represent halves of a superposition. The spectator atoms lead to additional phase diffusion through the s-wave collision. (d) Lattice depth dependence of γ_0. The bands are estimation of the contrast decay time. The gray band is $(\Gamma_{\text{nat}} + \Gamma_{\text{BBR}})/2$. The blue band is $(\Gamma_R + \Gamma_{\text{nat}} + \Gamma_{\text{BBR}})/2$. (e) Lattice depth dependence of γ_N. The band shows DDTWA simulations. The blue band includes the effect of spectator atoms, while the orange band excludes the interaction effect from the spectator atoms. The error bars show the 68% confidence interval.

different experimental conditions than ours. We could also attribute this small discrepancy to modeling imperfections such as assuming a constant temperature. The value of K_{ee} is consistent with a previous measurement [31].

Coherence time—We investigate the coherence time of the atomic ensembles using Ramsey interferometry. Because the coherence time of the atoms exceeds that of laser [37,38], the atom-laser phase is randomized at the readout. As a result, we repeat the experiment multiple times for a given dark time, T_{dark}, and measure the change in peak-to-peak excitation fraction as an estimate of the contrast, C. We subdivide the image of the atomic distribution [see also Fig. 3(a)] and take the average for each bin to estimate the atom number per site N_{site}. Large QPN can overestimate C; thus, we use only the bins where QPN corresponds to an excitation fraction noise $\lesssim 5\%$. We model the contrast decay trajectory [Fig. 2(a)] with an empirical stretched exponential, $C(T_{\text{dark}}) = C(0)\exp[-(\gamma T_{\text{dark}})^{\alpha}]$, where $\{C(0), \gamma, \alpha\}$ are the fit parameters, and γ represents the contrast decay rate. The fitted exponent α ranges from 0.7 to 1.3 across different lattice depths. The uncertainty is estimated via bootstrapping. The coherence time for an atom number per lattice site $N_{\text{site}} = 9$ is 118(9) s for $U_0 = 11E_r$, plotted as a black curve in Fig. 2(a).

The extracted γ shows a strong density dependence [Fig. 2(b)]. We fit the data to a linear curve, $\gamma = \gamma_0 + \gamma_N N_{\text{site}}$. Here, γ_0 represents the contrast decay rate at the single-atom regime, and γ_N quantifies the collisional interaction effect.

Figures 2(d) and 2(e) summarize the dependence of γ_0 and γ_N on U_0. γ_0 is dominated by the lattice Raman scattering rate $\Gamma_R(U) = \partial_U(\Gamma_e + \Gamma_L) \times U$, the single photon scattering rate from BBR $\Gamma_{\text{BBR}} \sim 1/164$ s^{-1}, and the natural lifetime of the excited state Γ_{nat}. We use the result from the previous section $\Gamma_R/U = 5.6(3) \times 10^{-4}$ s$^{-1}E_r^{-1}$. As shown in Fig. 2(d), γ_0 is mainly limited by Γ_R at high U_0 and converges to a value close to the sum of Γ_{nat} and Γ_{BBR} as U_0 approaches 0. We find that the observed γ_0 is captured by a simple estimation of $(\Gamma_R + \Gamma_{\text{nat}} + \Gamma_{\text{BBR}})/2$.

In contrast to γ_0, γ_N shows a nonmonotonic dependence on U_0 [Fig. 2(e)]. At shallow depths, delocalization between adjacent lattice sites introduces off-site s-wave interactions via spin-orbit coupling [18], which dominates the decoherence. As the lattice depth increases, the s-wave channel is suppressed, and the on site p-wave contribution grows with density. However, this effect does not explain the data quantitatively given the limited strength of p-wave interactions (the orange band).

Lattice Raman scattering introduces additional decoherence through the generation of spectator atoms [Fig. 2(c)]. The photon scattering events populate various nuclear spin states in g that are distinguishable from the clock state.

These spectator atoms interact with the clock atoms via strong on site s-wave collisions, becoming a dominant source of decoherence. In addition, the stochastic generation of the spectator atoms introduces further fluctuations in the clock phase [39]. These mechanisms are supported by theoretical simulations based on a dissipative discrete truncated Wigner approximation (DDTWA) [40]. In Fig. 2(e), we show the simulation result of γ_N with and without the spectator atoms. For deeper lattices, decoherence induced by spectator atoms becomes prominent, which limits the use of large atom numbers. We note that the simulation shows a nonlinear dependence of γ on N_{site} [40]. To account for this small nonlinearity, we fit the line for two different ranges, $[0, (2/3)\max(N_{\mathrm{site}})]$ and $[(1/3)\max(N_{\mathrm{site}}), \max(N_{\mathrm{site}})]$, and take the difference as additional uncertainties for γ_0 and γ_N. The same treatment is applied to the theoretical simulation when extracting γ_N, and its range is indicated by the bands. We exclude theoretical simulations for $U_0 > 10^2 E_r$ due to extra sources of decoherence in this regime such as atoms in higher bands not captured by our model.

Imaging spectroscopy—To estimate the atomic contribution for the clock instability beyond the laser coherence time, we perform a synchronous clock comparison by using a Ramsey protocol achieved through imaging spectroscopy [28]. The frequency difference of the two regions [Fig. 3(a)] is reflected as a correlation between the excitation fractions, resulting in a parametric plot with the shape of an ellipse [Fig. 3(b)]. The opening angle of the ellipse, ϕ, related to the frequency difference of the two regions is obtained from the ellipse fit. The QPN contribution to the variance of ϕ can be estimated as [28]

$$\mathrm{var}(\phi) = \frac{4}{C^2}\left(\int_0^{2\pi}\frac{d\theta}{2\pi}\frac{1}{\sum_{i=x,y}\csc^2(\theta_i)\mathrm{var}(p_i)}\right)^{-1}. \quad (2)$$

Here, $p_{x,y} = [1 + C\cos(\theta_{x,y})]/2$ represents the excitation fractions for each region with $\theta_{x,y} = \theta \mp \phi/2$, C is the contrast, θ is the phase of the laser, which is assumed to be uniformly distributed, and ϕ is the Ramsey phase difference between two regions [Fig. 3(a)]. For coherent spin states, the variance $\mathrm{var}(p_i) = p_i(1-p_i)/N_{\mathrm{ens}}$, where N_{ens} is the number of atoms in one ensemble. Note that Eq. (2) is a good approximation for the classical Cramér-Rao bound for large atom numbers and not so small ϕ [40,41]. The QPN contribution to the clock instability can be, therefore, estimated as

$$\sigma_y(\tau) = \frac{\sigma_y^{\mathrm{rel}}(\tau)}{\sqrt{2}} = \frac{\sqrt{\mathrm{var}(\phi)}}{2\pi\nu_0 T_{\mathrm{dark}}\sqrt{2\tau/T_{\mathrm{cycle}}}}, \quad (3)$$

where σ_y^{rel} is relative (comparison) instability between two regions, ν_0 is the frequency of the clock transition, T_{cycle} is the experimental cycle period, and τ is the averaging time. The reduction by a factor of $\sqrt{2}$ accounts for the independent contribution from the two regions.

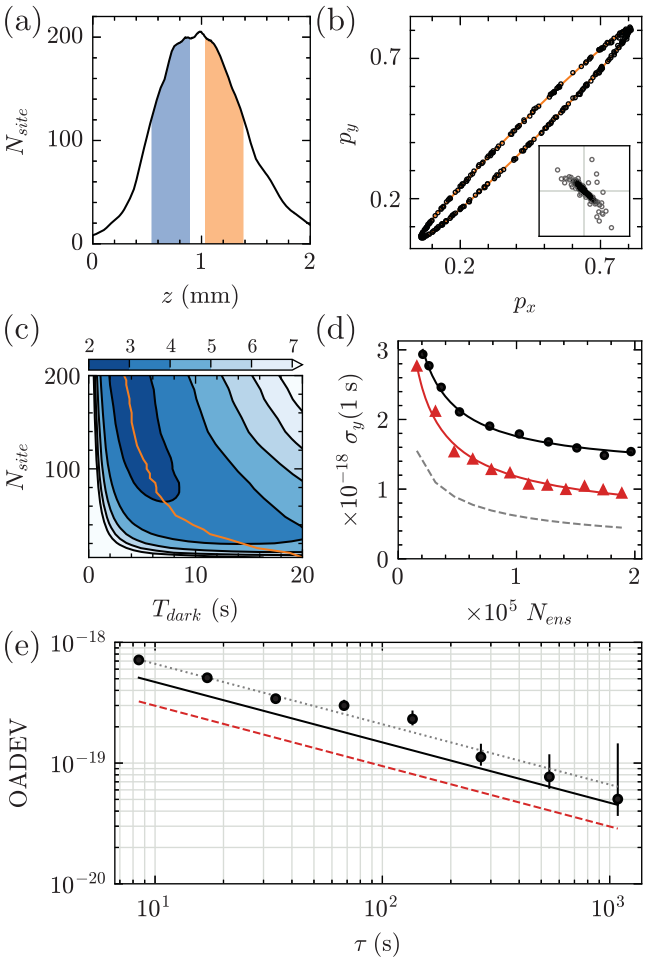

FIG. 3. Estimation of the atomic contribution to the clock stability. (a) 1D image of the atomic cloud. z is the coordinate along the gravity. The frequency difference between two regions (e.g., the blue and the orange) is induced by a magnetic field gradient of 12.7 mHz/mm. (b) Parametric plot of the excitation fractions of two regions. The black circles are the experimental data, and the orange solid line is the fitted ellipse. The inset shows the fit residuals, where each axis edge spans ± 0.01. The diagonal pattern is mostly from QPN. (c) A single lattice site's $\sigma_y(1\ \mathrm{s})$ in units of 10^{-17} as a function of N_{site} and T_{dark} from DDTWA. The orange line indicates the optimal T_{dark} as a function of N_{site}. (d) 1-s instability for different N_{ens}. The black circles are experimental data, and the red triangles are theoretical predictions. The solid lines are heuristic fits. The gray dashed line shows the theoretical prediction from Eq. (3) for coherent spin states. (e) Overlapping Allan Deviation (OADEV) for $\sigma_y(\tau)$. The black markers are comparison instability σ_y^{rel} and the gray line the fit. The black solid line is the single clock instability $\sigma_y(\tau) = 1.5 \times 10^{-18}/\sqrt{\tau/\mathrm{s}}$. The red dashed line is theoretical prediction. The error bars show the 68% confidence interval.

The contrast decay limits the achievable sensitivity with increasing T_{dark} and N_{site}. This competition results in a minimum instability at specific T_{dark} for a given T_{cycle} and N_{site}. Figure 3(c) presents such a parametric contour plot of $\sigma_y(\tau)$ based on DDTWA for $U_0 = 11E_r$ lattice depth at

which we see a minimal density-dependent contrast decay, and hence the best stability. The plot assumes a magnetic field gradient of 12.7 mHz/mm, a separation between adjacent lattice sites of 260 μm, and a phase accumulation ϕ linear with T_{dark}. The experimental dead time is accounted as $T_{\mathrm{cycle}} = T_{\mathrm{dark}} + 1.5$ s. The density profile of the sample [Fig. 3(a)] suggests using $T_{\mathrm{dark}} = 4$–8 s.

In Fig. 3(e), we present the Allan deviation for the comparison and a single clock instability, under $T_{\mathrm{dark}} = 7$ s and $T_{\mathrm{cycle}} = 8.48$ s with 313 realizations. A jackknifing method is used to generate series of ϕ and compute the Allan deviation [28]. Subsequently, we convert ϕ to σ_y^{rel}. The fit to data, $\propto 1/\sqrt{\tau}$ (the gray dotted line), along with a single clock $\sigma_y(1\ \mathrm{s}) = 1.5 \times 10^{-18}$ (the black solid line), is plotted with the theoretical QPN contribution for $\sigma_y(1\ \mathrm{s})$ of 9.4×10^{-19} (the red dashed line).

The observed instability is 50% larger than the theoretical estimate. To quantify the difference, we vary the bin size of the image [Fig. 3(a)] to change the atom number per ensemble, N_{ens}, and estimate the instability for each N_{ens} [Fig. 3(d)]. We observe that the experimental value starts to saturate after $N_{\mathrm{ens}} \approx 5 \times 10^4$. We fit a heuristic curve $\sigma_y(1\ \mathrm{s}) = \sqrt{a^2/N_{\mathrm{ens}} + b^2}$ to the data, where a and b are the fit parameters (solid lines). For the experimental data (black circles), $a = 5.57(9) \times 10^{-16}$, $b = 1.76(5) \times 10^{-18}$ and for the theoretical prediction (red triangles), $a = 4.8(1) \times 10^{-16}$, $b = 6.5(1.0) \times 10^{-19}$. This suggests that the observed instability is limited by an atom number-independent noise source, to be investigated in the future. We note that ellipse fitting can introduce additional noise and bias depending on the method [42–44]. We test the fitting method using simulated data; see [40] for more details. We also emphasize that the theoretically simulated σ_y (red) is larger than that predicted from coherent spin states (gray), indicating excess noise from the spectator atoms.

Conclusion—We report coherence time of 2 min for the ^{87}Sr clock transition in a shallow optical lattice. Through systematic investigations of various population decay mechanisms, we find that the observed coherence time in the single particle limit is consistent with predictions based on these mechanisms. When the atom number increases, we identify that spectator atoms with different spin states, generated via lattice Raman scattering, are essential for understanding the observed density-dependent decoherence rate. This density related decoherence cannot be canceled by balancing s- and p-wave contributions, unlike in the mean density shift [18]. To scale up the atom number for further improvement of precision, we, thus, need to increase the trapping volume and/or engineer favorable lattice site occupation. Guided by the understanding of the decoherence rates, we demonstrate instability from each ensemble of $1.5 \times 10^{-18}/\sqrt{\tau/\mathrm{s}}$, representing approximately a factor-of-2 improvement over the previous record [6]. Our findings advance the understanding of stability limits in state-of-the-art optical lattice clocks and pave the way for future developments in fundamental physics applications [5,45–47].

Note added—While performing this Letter, we became aware of related works [48,49], demonstrating the lifetime of the $^3P_0$ state and the extended coherence time with hyperfine state resolved readout in an OLC.

Acknowledgments—We thank A. Cao, A. Kaufman, and Y. Yang for useful discussions and review of this manuscript, and M. Miklos for discussion about ellipse fitting. Funding support is provided by NSF QLCI OMA-2016244, DOE National Quantum Information Science Research Centers—Quantum Systems Accelerator, V. Bush Fellowship, NSF JILA-PFC PHY-2317149, AFOSR FA9550-24-1-0179, and NIST.

Data availability—The data that support the findings of this Letter are available from the authors upon reasonable request.

[1] M. Takamoto, F.-L. Hong, R. Higashi, and H. Katori, An optical lattice clock, Nature (London) **435**, 321 (2005).
[2] M. M. Boyd, T. Zelevinsky, A. D. Ludlow, S. M. Foreman, S. Blatt, T. Ido, and J. Ye, Optical atomic coherence at the 1-second time scale, Science **314**, 1430 (2006).
[3] A. D. Ludlow, M. M. Boyd, J. Ye, E. Peik, and P. O. Schmidt, Optical atomic clocks, Rev. Mod. Phys. **87**, 637 (2015).
[4] N. Dimarcq *et al.*, Roadmap towards the redefinition of the second, Metrologia **61**, 012001 (2024).
[5] J. Ye and P. Zoller, Essay: Quantum sensing with atomic, molecular, and optical platforms for fundamental physics, Phys. Rev. Lett. **132**, 190001 (2024).
[6] T. Bothwell, C. J. Kennedy, A. Aeppli, D. Kedar, J. M. Robinson, E. Oelker, A. Staron, and J. Ye, Resolving the gravitational redshift across a millimetre-scale atomic sample, Nature (London) **602**, 420 (2022).
[7] X. Zheng, J. Dolde, M. C. Cambria, H. M. Lim, and S. Kolkowitz, A lab-based test of the gravitational redshift with a miniature clock network, Nat. Commun. **14**, 4886 (2023).
[8] M. Takamoto, I. Ushijima, N. Ohmae, T. Yahagi, K. Kokado, H. Shinkai, and H. Katori, Test of general relativity by a pair of transportable optical lattice clocks, Nat. Photonics **14**, 411 (2020).
[9] X. Zhang, M. Bishof, S. L. Bromley, C. V. Kraus, M. S. Safronova, P. Zoller, A. M. Rey, and J. Ye, Spectroscopic observation of su(n)-symmetric interactions in sr orbital magnetism, Science **345**, 1467 (2014).
[10] S. L. Bromley, S. Kolkowitz, T. Bothwell, D. Kedar, A. Safavi-Naini, M. L. Wall, C. Salomon, A. M. Rey, and J. Ye, Dynamics of interacting fermions under spin–orbit coupling in an optical lattice clock, Nat. Phys. **14**, 399 (2018).
[11] L. Sonderhouse, C. Sanner, R. B. Hutson, A. Goban, T. Bilitewski, L. Yan, W. R. Milner, A. M. Rey, and J. Ye,

Thermodynamics of a deeply degenerate su(n)-symmetric fermi gas, Nat. Phys. **16**, 1216 (2020).
[12] R. B. Hutson, W. R. Milner, L. Yan, J. Ye, and C. Sanner, Observation of millihertz-level cooperative Lamb shifts in an optical atomic clock, Science **383**, 384 (2024).
[13] W. R. Milner, S. Lannig, M. Mamaev, L. Yan, A. Chu, B. Lewis, M. N. Frankel, R. B. Hutson, A. M. Rey, and J. Ye, Coherent evolution of superexchange interaction in seconds-long optical clock spectroscopy, Science **388**, 503 (2025).
[14] J. M. Robinson, M. Miklos, Y. M. Tso, C. J. Kennedy, T. Bothwell, D. Kedar, J. K. Thompson, and J. Ye, Direct comparison of two spin-squeezed optical clock ensembles at the 10-17 level, Nat. Phys. **20**, 208 (2024).
[15] S. L. Campbell, R. B. Hutson, G. E. Marti, A. Goban, N. Darkwah Oppong, R. L. McNally, L. Sonderhouse, J. M. Robinson, W. Zhang, B. J. Bloom, and J. Ye, A Fermi-degenerate three-dimensional optical lattice clock, Science **358**, 90 (2017).
[16] I. S. Madjarov, A. Cooper, A. L. Shaw, J. P. Covey, V. Schkolnik, T. H. Yoon, J. R. Williams, and M. Endres, An atomic-array optical clock with single-atom readout, Phys. Rev. X **9**, 041052 (2019).
[17] M. A. Norcia, A. W. Young, W. J. Eckner, E. Oelker, J. Ye, and A. M. Kaufman, Seconds-scale coherence on an optical clock transition in a tweezer array, Science **366**, 93 (2019).
[18] A. Aeppli, A. Chu, T. Bothwell, C. J. Kennedy, D. Kedar, P. He, A. M. Rey, and J. Ye, Hamiltonian engineering of spin-orbit–coupled fermions in a Wannier-Stark optical lattice clock, Sci. Adv. **8**, eadc9242 (2022).
[19] R. B. Hutson, A. Goban, G. E. Marti, L. Sonderhouse, C. Sanner, and J. Ye, Engineering quantum states of matter for atomic clocks in shallow optical lattices, Phys. Rev. Lett. **123**, 123401 (2019).
[20] S. Dörscher, R. Schwarz, A. Al-Masoudi, S. Falke, U. Sterr, and C. Lisdat, Lattice-induced photon scattering in an optical lattice clock, Phys. Rev. A **97**, 063419 (2018).
[21] A. W. Young, W. J. Eckner, W. R. Milner, D. Kedar, M. A. Norcia, E. Oelker, N. Schine, J. Ye, and A. M. Kaufman, Half-minute-scale atomic coherence and high relative stability in a tweezer clock, Nature (London) **588**, 408 (2020).
[22] P. Niroula, J. Dolde, X. Zheng, J. Bringewatt, A. Ehrenberg, K. C. Cox, J. Thompson, M. J. Gullans, S. Kolkowitz, and A. V. Gorshkov, Quantum sensing with erasure qubits, Phys. Rev. Lett. **133**, 080801 (2024).
[23] G. K. Campbell, M. M. Boyd, J. W. Thomsen, M. J. Martin, S. Blatt, M. D. Swallows, T. L. Nicholson, T. Fortier, C. W. Oates, S. A. Diddams, N. D. Lemke, P. Naidon, P. Julienne, J. Ye, and A. D. Ludlow, Probing interactions between ultracold fermions, Science **324**, 360 (2009).
[24] P. Lemonde and P. Wolf, Optical lattice clock with atoms confined in a shallow trap, Phys. Rev. A **72**, 033409 (2005).
[25] S. Kolkowitz, S. L. Bromley, T. Bothwell, M. L. Wall, G. E. Marti, A. P. Koller, X. Zhang, A. M. Rey, and J. Ye, Spin–orbit-coupled fermions in an optical lattice clock, Nature (London) **542**, 66 (2016).
[26] K. Kim, A. Aeppli, T. Bothwell, and J. Ye, Evaluation of lattice light shift at low 10–19 uncertainty for a shallow lattice Sr optical clock, Phys. Rev. Lett. **130**, 113203 (2023).
[27] A. Aeppli, K. Kim, W. Warfield, M. S. Safronova, and J. Ye, Clock with 8×10-19 systematic uncertainty, Phys. Rev. Lett. **133**, 023401 (2024).
[28] G. E. Marti, R. B. Hutson, A. Goban, S. L. Campbell, N. Poli, and J. Ye, Imaging optical frequencies with 100 μHz precision and 1.1 μm resolution, Phys. Rev. Lett. **120**, 103201 (2018).
[29] H. Uys, M. J. Biercuk, A. P. VanDevender, C. Ospelkaus, D. Meiser, R. Ozeri, and J. J. Bollinger, Decoherence due to elastic Rayleigh scattering, Phys. Rev. Lett. **105**, 200401 (2010).
[30] R. Ozeri, C. Langer, J. D. Jost, B. L. DeMarco, A. Ben-Kish, B. R. Blakestad, J. Britton, J. Chiaverini, W. M. Itano, D. Hume, D. Leibfried, T. Rosenband, P. Schmidt, and D. J. Wineland, Hyperfine coherence in the presence of spontaneous photon scattering, Phys. Rev. Lett. **95**, 030403 (2005).
[31] M. Bishof, M. J. Martin, M. D. Swallows, C. Benko, Y. Lin, G. Quéméner, A. M. Rey, and J. Ye, Inelastic collisions and density-dependent excitation suppression in a 87Sr optical lattice clock, Phys. Rev. A **84**, 052716 (2011).
[32] I. Ushijima, M. Takamoto, and H. Katori, Operational magic intensity for Sr optical lattice clocks, Phys. Rev. Lett. **121**, 263202 (2018).
[33] M. Yasuda and H. Katori, Lifetime measurement of the P 2 3 metastable state of strontium atoms, Phys. Rev. Lett. **92**, 153004 (2004).
[34] M. M. Boyd, T. Zelevinsky, A. D. Ludlow, S. Blatt, T. Zanon-Willette, S. M. Foreman, and J. Ye, Nuclear spin effects in optical lattice clocks, Phys. Rev. A **76**, 022510 (2007).
[35] X.-T. Lu, F. Guo, Y.-Y. Liu, J.-J. Xia, G.-D. Zhao, Y.-X. Chen, Y.-B. Wang, B.-Q. Lu, and H. Chang, Determining the lifetime of the 5 s 5 p 3 P 0 o metastable state in 87 Sr from the electric dipole matrix element, Phys. Rev. Appl. **21**, 024042 (2024).
[36] J. A. Muniz, D. J. Young, J. R. K. Cline, and J. K. Thompson, Cavity-QED measurements of the Sr 87 millihertz optical clock transition and determination of its natural linewidth, Phys. Rev. Res. **3**, 023152 (2021).
[37] E. Oelker, R. B. Hutson, C. J. Kennedy, L. Sonderhouse, T. Bothwell, A. Goban, D. Kedar, C. Sanner, J. M. Robinson, G. E. Marti, D. G. Matei, T. Legero, M. Giunta, R. Holzwarth, F. Riehle, U. Sterr, and J. Ye, Demonstration of 4.8×10-17 stability at 1 s for two independent optical clocks, Nat. Photonics **13**, 714 (2019).
[38] D. G. Matei, T. Legero, S. Häfner, C. Grebing, R. Weyrich, W. Zhang, L. Sonderhouse, J. M. Robinson, J. Ye, F. Riehle, and U. Sterr, 1.5 μm lasers with Sub-10 mHz linewidth, Phys. Rev. Lett. **118**, 263202 (2017).
[39] Y. Li, K. Pawłowski, B. Décamps, P. Colciaghi, M. Fadel, P. Treutlein, and T. Zibold, Fundamental limit of phase coherence in two-component Bose-Einstein condensates, Phys. Rev. Lett. **125**, 123402 (2020).
[40] See Supplemental Material at http://link.aps.org/supplemental/10.1103/3wtv-sty2 for more information.
[41] L. Pezzè, A. Smerzi, M. K. Oberthaler, R. Schmied, and P. Treutlein, Quantum metrology with nonclassical states of atomic ensembles, Rev. Mod. Phys. **90**, 035005 (2018).
[42] R. Corgier, M. Malitesta, L. A. Sidorenkov, F. P. D. Santos, G. Rosi, G. M. Tino, A. Smerzi, L. Salvi, and L. Pezzè, Optimized squeezing for accurate differential sensing under

large phase noise, Quantum Sci. Technol. **10**, 045016 (2025).

[43] J. K. Stockton, X. Wu, and M. A. Kasevich, Bayesian estimation of differential interferometer phase, Phys. Rev. A **76**, 033613 (2007).

[44] W. J. Eckner, N. Darkwah Oppong, A. Cao, A. W. Young, W. R. Milner, J. M. Robinson, J. Ye, and A. M. Kaufman, Realizing spin squeezing with Rydberg interactions in an optical clock, Nature (London) **621**, 734 (2023).

[45] A. Chu, V. J. Martínez-Lahuerta, M. Miklos, K. Kim, P. Zoller, K. Hammerer, J. Ye, and A. M. Rey, Exploring the dynamical interplay between mass-energy equivalence, interactions, and entanglement in an optical lattice clock, Phys. Rev. Lett. **134**, 093201 (2025).

[46] S. Kolkowitz, I. Pikovski, N. Langellier, M. D. Lukin, R. L. Walsworth, and J. Ye, Gravitational wave detection with optical lattice atomic clocks, Phys. Rev. D **94**, 124043 (2016).

[47] M. Zych, F. Costa, I. Pikovski, and Č. Brukner, Quantum interferometric visibility as a witness of general relativistic proper time, Nat. Commun. **2**, 505 (2011).

[48] J. Dolde, D. Ganapathy, X. Zheng, S. Ma, K. Beloy, and S. Kolkowitz, Direct measurement of the 3P0 clock state natural lifetime in 87Sr, arXiv:2505.06440.

[49] S. Ma, J. Dolde, X. Zheng, D. Ganapathy, A. Shtov, J. Chen, A. Stoeltzel, and S. Kolkowitz, Enhancing optical lattice clock coherence times with erasure conversion, arXiv:2505.06437.